

We attribute the high thermal stability of the hcp inclusion compounds $[(T_{\text{on}} - T_{\text{b}}): 2\cdot\text{CF}_3\text{Br}, 260^\circ\text{C}; 2\cdot\text{CF}_4, 370^\circ\text{C}; 2\cdot\text{CH}_4, 320^\circ\text{C}]$ to the host lattice being isomorphous with its pure phase—the host lattice cannot gain much stability by releasing the guest because the initial and final lattices would be identical, even at elevated temperatures. In contrast to the zeolites, the guest cannot easily diffuse through the host lattice because the channels are nonporous.

The stabilization of volatile species in a solid matrix purely by van der Waals forces is not without precedent: An argon inclusion compound of the approximately spherical molecule tetra-*tert*-butyltetrahedrane has been reported (20). This complex also crystallizes as a hcp array of host molecules with the argon guest situated in interstitial voids (space group $P6_3/m$, $a = 15.73\text{\AA}$, $c = 13.92\text{\AA}$). However, the complex is only stable below about -50°C . Above this temperature, the guest is released and the host lattice is destroyed. In sharp contrast, we have shown that $2\cdot\text{CF}_4$ is stable up to 240°C . To account for this extreme difference in stability between the two seemingly analogous structures, we carefully examined the host-guest packing modes. The most notable difference between the two inclusion systems is that the guest-containing voids of the argon inclusion compound are formed by periodic dilation of type **a** channels, whereas the type **b** channels are constricted. On the basis of this observation, we propose that, to stabilize highly volatile guests in a hexagonal crystal system, the guest molecules should reside within a void fashioned from a type **b** channel. An approach to designing suitable host matrices based on the principles of crystal engineering would thus involve a judicious choice of host such that its geometry would facilitate enlargement of type **b** channels and shrinking of type **a** channels.

References and Notes

1. A. J. Kitaigorodsky, *Mixed Crystals* (Springer Series in Solid-State Sciences 33, Springer-Verlag, Berlin, 1984).
2. A. Gavezzotti, Ed., *Theoretical Aspects and Computer Modeling of the Molecular Solid State* (Wiley, Chichester, UK, 1997).
3. A. J. Kitaigorodsky, *Molecular Crystals and Molecules* (Academic Press, New York, 1973).
4. J. L. Atwood, J. E. D. Davies, D. D. MacNicol, F. Vögtle, Eds., *Comprehensive Supramolecular Chemistry* (Elsevier Science, Oxford, 1996), vols. 1–11.
5. D. E. Palin, H. M. Powell, *Nature* **156**, 334 (1945).
6. A. P. Dianin, *J. Russ. Phys. Chem. Soc.* **46**, 1310 (1914).
7. D. D. MacNicol, in *Inclusion Compounds*, J. L. Atwood, J. E. D. Davies, D. D. MacNicol, Eds. (Academic Press, London, 1984), vol. 2.
8. C. D. Gutsche, *Calixarenes*, J. F. Stoddart, Ed. (Royal Society of Chemistry, London, 1989).
9. L. R. MacGillivray, J. L. Atwood, *Nature* **389**, 469 (1997).
10. J. L. Atwood, L. J. Barbour, A. Jerga, *Chem. Commun.* 2376 (2001).
11. ———, *J. Am. Chem. Soc.* **124**, 2122 (2002).

12. G. W. Orr, L. J. Barbour, J. L. Atwood, *Science* **285**, 1049 (1999).
13. R. Ungaro, A. Pochini, G. D. Andreotti, V. Sangermano, *J. Chem. Soc. Perkin Trans. 2*, 1979 (1984).
14. H. Akdas *et al.*, *Tetrahedron Lett.* **39**, 2311 (1998).
15. P. Zhang, Z. Huang, *Huaxue Xuebao* **50**, 209 (1992).
16. J. M. Harrowfield, M. I. Ogden, W. R. Richmond, B. W. Skelton, A. H. White, *J. Chem. Soc. Perkin Trans. 2*, 2183 (1993).
17. *Comprehensive Supramolecular Chemistry*, J. L. Atwood, J. E. D. Davies, D. D. MacNicol, F. Vögtle, Eds. (Elsevier Science, Oxford, 1996), vol. 9.
18. M. R. Caira, T. le Roux, L. R. Nassimbeni, *Chem. Commun.* 2128 (2001).
19. M. R. Caira, L. R. Nassimbeni, in *Comprehensive Supramolecular Chemistry*, J. L. Atwood, J. E. D. Davies, D. D. MacNicol, F. Vögtle, Eds. (Elsevier Science, Oxford, 1996), vol. 6.
20. H. Irgartinger, R. Jahn, G. Maier, R. Emrich, *Angew. Chem. Int. Ed. Engl.* **26**, 356 (1987).
21. We thank the National Science Foundation for support of this work.

26 March 2002; accepted 30 April 2002

Published online 9 May 2002;

10.1126/science.1072252

Include this information when citing this paper.

Conformational Dynamics in a Dipeptide After Single-Mode Vibrational Excitation

Brian C. Dian, Asier Longarte, Timothy S. Zwier*

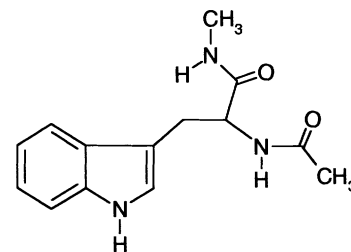
The dynamics of conformational isomerization are explored in a methyl-capped dipeptide, *N*-acetyl-tryptophan methyl amide (NATMA), using infrared-ultraviolet (IR-UV) hole-filling and IR-induced population transfer spectroscopies. IR radiation selectively excites individual NH stretch vibrational fundamentals of single conformations of the molecule in the early portions of a gas-phase expansion, and then this excited population is collisionally recooled into its conformational minima for subsequent conformation-specific detection. Efficient isomerization is induced by the IR excitation that redistributes population between the same conformations that have population in the absence of IR excitation. The quantum yields for transfer of the population into the various conformational minima depend uniquely on which conformation is excited and on which NH stretch vibration is excited within a given conformation.

Experimental studies of the mechanisms and dynamics of conformational isomerization in flexible molecules are faced with very different tasks, depending on the size of the molecule of interest. In the simplest case, two conformational minima are separated by a single transition state involving motion along a well-defined reaction coordinate (e.g., *cis/trans* isomerization in $\text{XHC}=\text{CHY}$) (1). Large macromolecules undergo conformational change on a potential energy landscape that involves millions of conformational minima and an even greater number of pathways connecting them (2, 3). Between these two extremes lies an interesting size regime in which the conformational landscape exhibits considerable complexity, but selective excitation and detection of single conformations are still possible. Furthermore, precise amounts of energy can be placed in the molecule in well-defined initial vibrations, enabling mode-specific effects to be probed. Here we describe initial results from a laser-based, IR-UV pump-probe method that can be applied with considerable precision to

study conformational isomerization and energy flow in isolated molecules in this intermediate-size regime.

We chose for our initial study *N*-acetyl-tryptophan methyl amide (NATMA), a methyl-capped dipeptide. An exhaustive search of the conformational space of this molecule with the AMBER force field (4) reveals that it has 164 minima connected by 714 transition states (5). There are 65 conformational minima calculated to lie within 40 kJ/mol of the global minimum. The conformational minima of NATMA can be categorized into “families” of structures that share a common dipeptide backbone configuration (6).

The three lowest-energy conformers of



N-acetyl-tryptophan methyl amide, NATMA
Structure 1.

Department of Chemistry, Purdue University, West Lafayette, IN 47907–1393, USA.

*To whom correspondence should be addressed. E-mail: zwier@purdue.edu

NATMA are shown in Fig. 1A. Two of these structures [A(C5) and B(C5)] belong to a "C5" family with extended dipeptide backbones that differ in the orientation of the indole ring relative to the backbone. The third conformer [C(C7)] belongs to a second family ("C7") that contains an intramolecular hydrogen bond between the exterior NH group of one peptide unit and the carbonyl group on the other, forming a seven-membered ring. NATMA incorporates an indole molecule into its side chain, which makes it possible to detect NATMA with high sensitivity in the UV ($\sim 35,000\text{ cm}^{-1}$) with laser-induced fluorescence (LIF) (7).

We have recently studied the conformational preferences of NATMA using double-resonance laser spectroscopy to record IR and UV spectra of single conformations of the molecule free from interference from one another (8). A supersonic expansion cooled the NATMA molecules into the zero-point

levels of several of the lowest-energy conformational minima. Only three conformations with detectable population were observed (Fig. 1A). These studies also provided the IR spectral signatures for the NH stretch vibrations of the amide NH groups in the peptide backbones of the three conformations.

The experiments described here build on this foundation to study the dynamics of conformational isomerization. A schematic diagram of the spatial and timing requirements for the method is shown in Fig. 1B, and an energy-level diagram for the methods is shown in Fig. 1C. The NATMA sample is heated to 150°C to obtain sufficient vapor pressure, entrained in several atmospheres of helium, and pulsed through a 0.8-mm-diameter orifice into a vacuum chamber to create a supersonic expansion. A distinguishing feature of the hole-filling technique is the spatial separation of the IR and UV laser beams. In the method used here, IR excitation occurs

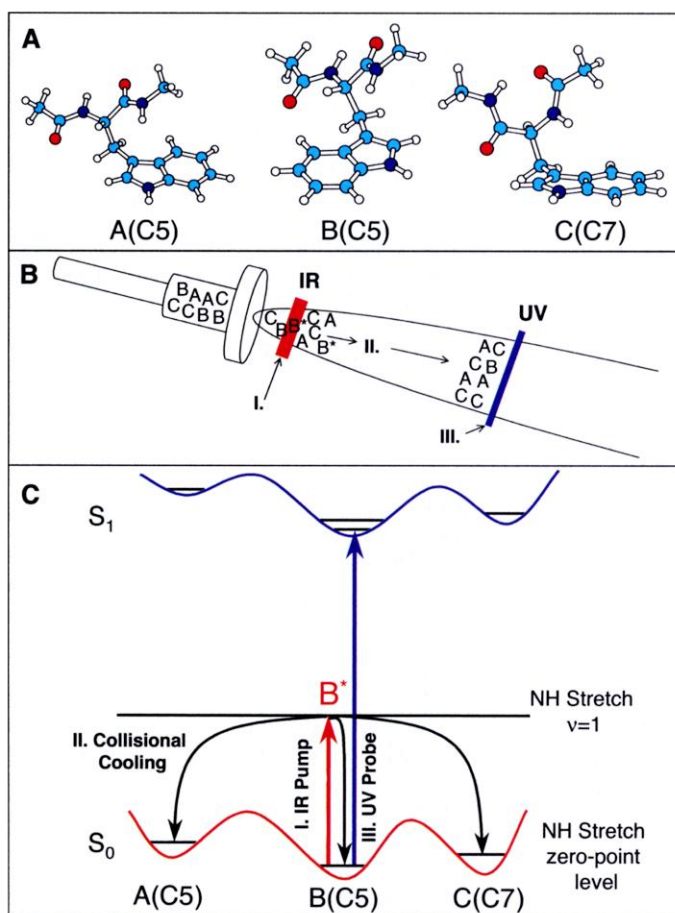
early in the supersonic expansion ($\sim 1\text{ mm}$ from the expansion orifice) rather than in the collision-free region downstream. An IR wavelength is chosen such that only a single conformation absorbs through an NH stretch frequency unique to a particular NH group of that conformer. The conformation that absorbs the IR radiation has a fraction of its population receiving this additional energy ($\sim 40\text{ kJ/mol}$), thereby creating a "hole" in its ground-state population. This additional energy is available to the excited molecules for conformational isomerization. By exciting molecules early in the expansion, many collisions occur after IR excitation to cool the excited molecules into the zero-point levels of the conformational minima accessible to them. The redistributed conformational population is then probed about $2\ \mu\text{s}$ later in the collision-free region of the expansion ($\sim 4\text{ mm}$ downstream), by using LIF to excite the ground-to-first excited singlet state electronic transitions of the conformers.

Two complementary schemes were used. In "IR-UV hole-filling spectroscopy," the IR pump laser was fixed to a specific NH stretch fundamental of a particular conformation of NATMA, and the UV probe laser was tuned over the S_1 - S_0 origin region of the conformations (Fig. 1B). The energy that was initially introduced into this conformation through a specific IR absorption relaxed intramolecularly and collisionally, either back to the initially excited conformational minimum or over isomerization barriers into different conformational minima. The difference in LIF signal with and without the IR laser present reflected the change in population of the various conformers. The conformation chosen for excitation had its UV transitions appearing as a depletion in the hole-filling scan, whereas the UV transitions due to the conformations gaining population showed up as gain signals.

Alternatively, in IR-induced population transfer spectroscopy (IRPTS), the IR excitation laser was tuned while the UV laser was held fixed on a particular transition in the LIF spectrum, thereby serving as a monitor of the population of that conformer. The resulting IR spectrum then reflected the population changes induced by the upstream IR laser on the downstream population of a given conformer.

The LIF spectrum of NATMA in the region of the S_0 - S_1 electronic origin (Fig. 2A) contains contributions from all three conformers present in the expansion. UV-UV hole-burning spectroscopy (8, 9) was then used to dissect the LIF spectrum into its contributions from each of the conformations present in the expansion. The inset in Fig. 2A shows three UV-UV hole-burning scans that identify the transitions due to conformers A(C5), B(C5), and C(C7) in the LIF spec-

Fig. 1. (A) Structures of the three lowest-energy conformers of *N*-acetyl-tryptophan methyl amide (NATMA). These three structures are the only ones observed in the supersonic expansion. Schematic diagram of the (B) spatial and temporal arrangement, and (C) energy-level diagram for the IR-UV hole-filling and IR population transfer spectroscopy (IRPTS) experiments. NATMA molecules are entrained in three bars of helium and expanded through a 0.8-mm-diameter orifice of a pulsed valve, operating at 20 Hz, into a vacuum chamber pumped by a roots blower. The conformers of NATMA begin to cool, before being excited with an IR light pulse from an optical parametric converter. Selective excitation of one of the NH stretch fundamentals of a single conformer (e.g., conformer B) with the IR pulse gives these excited B conformers 40 kJ/mol of excess energy and creates a hole in the population of its zero-point level. Collisional cooling in the expansion (II) removes this excess energy, partially refilling the original conformer B(C5) minimum or producing a gain in population in other conformers [A(C5) or C(C7)]. A UV laser pulse (III), timed to intercept the recooled molecules ($\sim 2\ \mu\text{s}$ delay from the IR pulse), probes the resulting population changes induced by the IR source. In IR-UV hole-filling spectroscopy, the IR is fixed in wavelength, and the UV laser is tuned. These scans probe where the excited population went. In IRPTS, the IR is tuned, while the UV laser is fixed on a unique transition due to one of the conformers. IRPTS probes the population transfer into and out of a given conformational minimum. In either case, the IR light is pulsed only every other time the UV laser fires, and the difference in LIF signal from the UV laser is recorded.



trum. The UV spectrum of conformer C differs from that of A and B, but for our purposes here, this is of little consequence.

In the hole-filling scan shown in Fig. 2B, the IR laser was fixed at 3454 cm^{-1} , which selects for excitation of conformer B through its ψ -amide NH stretch fundamental. The creation of a "hole" in conformer B's ground-state zero-point level population produces a "dip" in the LIF signal for its transitions, whereas gain signals are observed in the LIF transitions of conformers A and C due to population transfer into these minima. The recoiling is complete, because no evidence for hot bands is present in the gain signal. Other hole-filling spectra (not shown) demonstrate selective excitation of conformers C and A, depending on the IR wavelength selected. Thus, by proper choice of IR wavelength, we can selectively excite a single conformer and create new conformational population distributions downstream in the expansion.

Quantitative information regarding the transfer of population is best obtained by using IRPTS. The red traces in Fig. 3, A to C, show a series of IRPT spectra recorded with the UV probe laser fixed on transitions that selectively monitor the fluorescence from A(C5), B(C5), and C(C7), respectively. The black traces below the IRPT spectra were recorded with the pulsed valve pulled back to a position in which cooling collisions no longer occur between IR absorption and UV probe. Under these conditions, only the IR depletions of each of the three conformers were observed. These spectra identify the unique IR transitions of each conformer [3440 and 3466 cm^{-1} for A(C5), 3431 and 3454 cm^{-1} for B(C5), 3342 cm^{-1} and 3429 cm^{-1} for C(C7)]. The IRPT spectra (red traces) have broader IR absorptions than the "zero-filling" spectra (black traces) because IR excitation occurs in a warmer part of the expansion for the former scans, where rotational cooling is not yet complete.

The NH stretch fundamentals in this IR wavelength region are due to localized stretches of the amide and indole NH bonds. The NH bonds responsible for each IR transition in Fig. 3 are indicated in the structures in Fig. 4. All traces in Fig. 3 are plotted as fractional depletions on the ordinate axis, which corresponds to the fractional change in the ground-state population of the conformer being monitored.

Certain bands in the IRPT spectra, such as the transitions at 3440 cm^{-1} and 3466 cm^{-1} in A, 3454 cm^{-1} in B, and 3342 cm^{-1} in C, are well separated from other bands and can produce a population dip in the conformer responsible for the absorption and corresponding gains in the populations of the other two conformers. Other transitions (3429 and 3431 cm^{-1} in B and C), which show partial

overlap with one another, produce more complicated profiles that reflect the competition between gain and depletion in these regions.

The IR-UV hole-filling spectra show no evidence for the formation of new conformations. Because the entire excited population is cooled back to the zero-point levels of conformers A, B, and C, the total net change in population in the three conformers, $\Delta N_A + \Delta N_B + \Delta N_C$, must be zero at all IR wavelengths. This criterion can be used to find the initial fractional populations of the three conformers (i.e., in the absence of the IR excitation). As shown in Fig. 3D, such a condition is met with fractional populations of conformers A(C5), B(C5), and C(C7): $F_A = 0.23$, $F_B = 0.40$, and $F_C = 0.37$, where F_N represents the N th conformer's fraction of the total NATMA population.

The "zero-filling" spectra of Fig. 3 show depletions that measure the fraction of the population of a given conformer excited at that IR wavelength. When combined with the IRPT spectra taken under identical laser conditions, a quantitative measure of how this excited population redistributes itself can be obtained for each unique IR absorption. For example, for the IR transition at 3342 cm^{-1} , which is due to conformer C(C7), we define Φ_{CA} as the quantum yield (10) for formation of conformer A downstream after excitation of conformer C upstream. If all of the C conformers excited by the laser were to cool back into the same minimum, then $\Phi_{CC} = 1$,

and $\Phi_{CA} = \Phi_{CB} = 0$. In that case, the dip in "C" would be completely filled in by the cooling collisions, and no gains would appear in the spectra of A or B. Clearly, the spectra of Fig. 3 do not conform to this limiting case.

The dotted traces that overlay the experimental IRPT spectra of Fig. 3 are the net result of fitting the regions around the six IR absorptions to extract six sets of quantum yields, one set for each of the two amide NH stretch fundamentals of the three conformers. The details of the fitting scheme will be described elsewhere (8). The fits successfully reproduce the complex band shapes arising from the convoluted sets of dips and gains present in each of the three action spectra, leading to unique sets of quantum yields for each transition.

The resulting measurements of the quantum yields for the six vibrational fundamentals are summarized in Fig. 4. Several important conclusions can be drawn from the data. First, isomerization by this means is efficient. The method can be used to create new conformational distributions downstream in the expansion that differ substantially from those created in the absence of the IR radiation. One could thus imagine using this pump-and-cool scheme to study the conformational dependence of photo-induced or bimolecular reactions by systematically varying the conformational distribution. Second, the isomerizations induced by the IR radiation involve large structural changes, breaking or forming

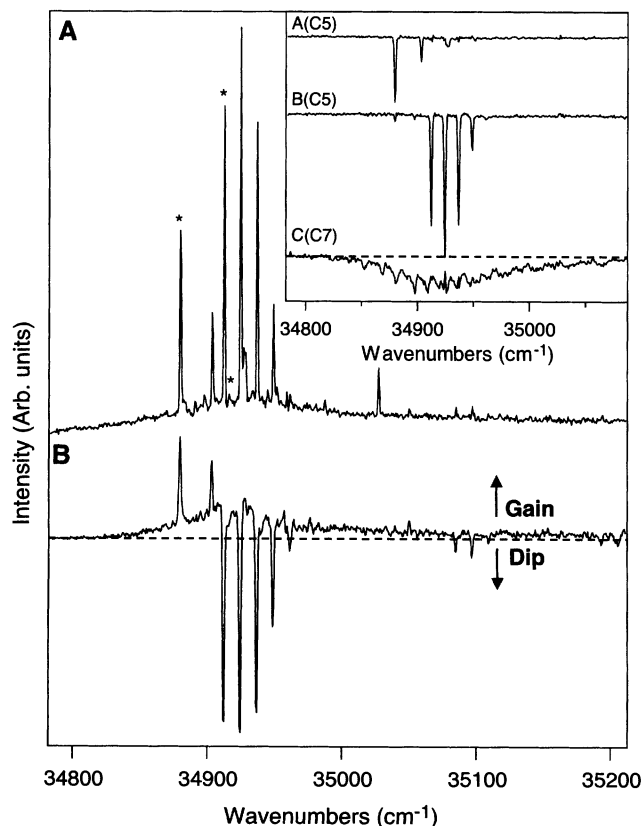
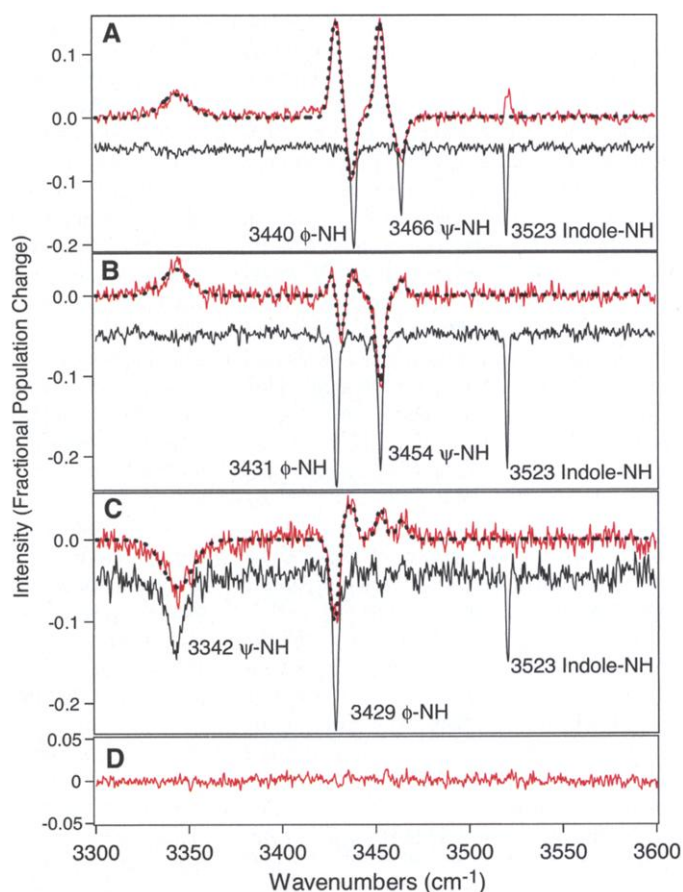


Fig. 2. (A) Laser-induced fluorescence (LIF) excitation spectrum of NATMA in the region of the S_0 - S_1 origin. The LIF spectrum contains contributions from all conformers present in the expansion. The inset shows three UV-UV hole-burning scans that separate the LIF spectrum into its constituent parts, identifying three conformers, A, B, and C. (B) IR-UV hole-filling spectrum with the IR source tuned to 3454 cm^{-1} , at the peak of the ψ -amide NH stretch of conformer B. Selective excitation of B appears as a dip in the fluorescence signal for the transitions due to B, while gain signals are observed in transitions assignable to A and C.

Fig. 3. (A to C) IRPT spectra (red traces) monitoring UV transitions marked with an asterisk in Fig. 2A, due to A(C5), B(C5), and C(C7) conformers. The corresponding "zero-filling" spectra are shown as black traces, recorded under identical conditions, but with the pulsed valve pulled back to a position where insufficient cooling collisions occur between the IR pump and UV probe lasers to refill the zero-point levels of the conformers. In that case, only depletions are observed that provide a measure of the fraction of the population excited with the IR laser. The wavenumber positions (in cm^{-1}) and assignments for the NH stretch fundamentals are given next to the transitions in the "zero-filling" spectra. (D) Weighted sum of the red traces used to determine the fractional abundances of conformers A, B, and C in the absence of the IR. The trace shown is for $F_A = 0.23 \pm 0.02$, $F_B = 0.40 \pm 0.02$, and $F_C = 0.37 \pm 0.02$, where F_N represents the N th conformer's fraction of the total NATMA population. At all IR wavelengths, this weighted sum must give zero net gain or depletion if no net loss in population occurs in the experiment.



an intramolecular hydrogen bond [C(C7) to A(C5) or B(C5)] or reconfiguring the indole side chain relative to the peptide backbone [A(C5) to B(C5)]. Third, in NATMA, the new distributions involve a redistribution of population among the conformations already having population in them but do not trap population in new minima, despite the presence of about 60 minima that are energetically accessible immediately after IR excitation. Preliminary results on two other molecules lead to similar conclusions (11), but additional examples are needed before a firm generalization can be drawn. Of most importance, the quantum yields for formation of the three conformers vary widely from one transition to the next. Given that the three conformers have a similar energy (within ~ 2 kJ/mol) and receive nearly identical amounts of energy in the vibrational excitation, one might have imagined that all transitions out of the three conformers would distribute their excited population similarly. As shown in Fig. 4, this is clearly not the case.

Indeed, the quantum yields are both conformation specific and mode specific. An example of the former is provided by a comparison of the 3466 cm^{-1} transition in A and the 3454 cm^{-1} transition in B(C5). Both involve excitation of the ψ -amide NH stretch. Excitation of these structurally equivalent (but conformationally inequivalent) NH groups leads to completely different quantum yields for population transfer. When A(C5) is excited it preferentially forms C(C7) (where an intramolecular H-bond is formed); when B(C5) is excited it preferentially forms A(C5).

The most notable example of vibrational mode-selectivity is the qualitatively different quantum yield distributions produced by excitation of the two amide NH stretch fundamentals of conformer B. When the ψ -amide NH stretch is excited (3454 cm^{-1}), conformer A is produced efficiently (Φ_{BA} large), whereas excitation of the ϕ -amide NH (3431 cm^{-1}) produces little A, but instead re-forms B with high yield. Similarly, isomerization out of the conformer A well is substantially more efficient when the ψ -amide NH (3466 cm^{-1} , $\Phi_{AA} = 0.04 \pm 0.04$), rather than the ϕ -amide NH (3440 cm^{-1} , $\Phi_{AA} = 0.28 \pm 0.03$), is excited. These results indicate that unique pathways on the potential energy surface play a critical role in dictating the redistribution of population under the circumstances of the present experiment. Alternatively, when the H-bonded NH stretch of conformer C(C7) is excited, a quantum yield distribution similar to the starting population distribution is produced, suggesting that the $\text{NH} \cdots \text{O}=\text{C}$ H-bond may facilitate more complete energy redistribution throughout the dipeptide backbone. In a similar way, nonselective excitation of all three indole NH

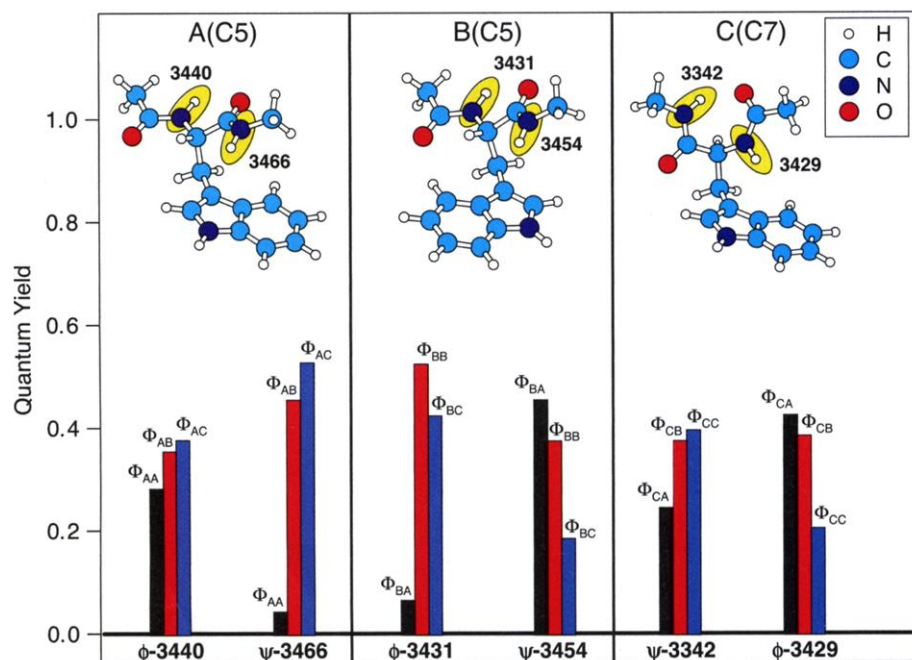


Fig. 4. Quantum yields for isomerization following IR excitation of the indicated NH stretch fundamentals. Φ_{ij} is the quantum yield for formation of conformer J following IR excitation of conformer I. Typical error bars on the quantum yields are ± 0.03 .

stretch fundamentals (which overlap at 3523 cm^{-1}) produces little net change in the population of the three conformations, consistent with their position remote from the dipeptide backbone.

The observation of vibrational mode-selectivity in the conformational isomerization of a molecule of this size is an unexpected result. Many previous studies on much smaller molecules have concluded that vibrationally mode-specific behavior is increasingly unlikely as the size of the molecule increases (12, 13). Intramolecular vibrational redistribution, or vibrational state mixing, increases with increasing molecular size because the density of vibrational states at a given energy rises quickly with increasing molecular size, washing out mode-specific excitation by diluting the make-up of the state carrying the oscillator strength with an increasing number of background levels at that energy.

However, the present experiment probes conformational isomerization rather than bond breaking, with barriers separating the conformational minima of about 20 kJ/mol, total excitation energies of only about 40 kJ/mol, and fast cooling in the expansion (with the first cooling collision on the 10^{-10} s time scale). Such conditions could limit the extent to which energy can redistribute throughout the molecule before trapping behind a barrier to isomerization. If the molecule is large enough, the parts of the molecule far from the point of excitation should play little role in the dynamics that follow IR excitation. In this sense, vibrational mode-selectivity may be more readily achieved in very large molecules than in small ones, if selective excitation can be achieved. In addition, the cooling collisions may participate in changing the conformational populations rather than simply quenching them. Thus, in the presence of competing deactivation, the kinds of conformational change that can be induced by IR excitation may have a characteristic length scale that the present experiment could be beginning to explore, pointing to the need for further experiments of this kind, supported by theory.

References and Notes

- V. C. Vachev, J. H. Frederick, B. A. Brishanin, V. N. Zadkov, N. I. Koroteev, *J. Phys. Chem.* **99**, 5247 (1995).
- F. M. Richards, in *Protein Folding*, T. E. Creighton, Ed. (Freeman, New York, 1992), pp. 1–58.
- P. N. Mortenson, D. J. Wales, *J. Chem. Phys.* **114**, 6443 (2001).
- W. D. Cornell, et al., *J. Am. Chem. Soc.* **117**, 5179 (1995).
- D. Evans, D. J. Wales, personal communication.
- T. Head-Gordon, M. Head-Gordon, M. J. Frisch, C. L. Brooks III, J. A. Pople, *J. Am. Chem. Soc.* **113**, 5989 (1991).
- M. J. Tubergen, J. R. Cable, D. H. Levy, *J. Chem. Phys.* **92**, 51 (1990).
- B. C. Dian, A. Longarte-Aldamo, S. Mercier, T. S. Zwier, in preparation.
- T. S. Zwier, *J. Phys. Chem. A* **105**, 8827 (2001).
- These measurements are equivalent to a photochemical quantum yield measurement. Photoexcitation of conformer I produces a certain population of excited molecules. The quantum yield Φ_{ij} is then the fraction of this excited population of conformer I that ends up as conformer j.
- On the basis of preliminary results from *N*-acetyltryptophan amide and melatonin.
- D. J. Nesbitt, R. W. Field, *J. Phys. Chem.* **100**, 12735 (1996).
- F. F. Crim, *J. Phys. Chem.* **100**, 12725 (1996).
- We acknowledge the National Science Foundation and the Petroleum Research Fund for support of this research (grant CHE-9728636). A.L. acknowledges the MCYT for his postdoctoral fellowship.

Published online 23 May 2002;
10.1126/science.1071563

Include this information when citing this paper.

6 March 2002; accepted 15 May 2002

Nitrate Controls on Iron and Arsenic in an Urban Lake

David B. Senn*† and Harold F. Hemond

Aquatic ecosystems are often contaminated by multiple substances. Nitrate, a common aquatic pollutant, strongly influenced the cycling of arsenic (As) under anoxic conditions in urban Upper Mystic Lake (Massachusetts, USA) by oxidizing ferrous iron [Fe(II)] to produce As-sorbing particulate hydrous ferric oxides and causing the more oxidized As(V), which is more particle-reactive than As(III) under these conditions, to dominate. This process is likely to be important in many natural waters.

Arsenic cycling in aquatic systems is strongly influenced by redox processes. For example, oxidized [arsenate, $\text{H}_2\text{As}^{(\text{V})}\text{O}_4^-$] and reduced [arsenite, $\text{H}_3\text{As}^{(\text{III})}\text{O}_3^-$] forms of inorganic As can differ both in their tendency to form soluble or insoluble complexes (1–3) and in their toxicity to humans and aquatic communities (1). Moreover, because surface complexation of As by solid hydrous ferric oxide (HFO; Fe in the +III oxidation state) often plays a dominant role in immobilizing As (2, 3), redox processes that affect Fe speciation can also have a strong indirect effect on As (4). Thus, redox-active pollutants (oxidants or reductants) could have the potential to affect As mobility. Nitrogen (N) pollution, arising from activities such as agricultural fertilization and fuel combustion, is generally of concern for its roles in eutrophication and acidification (5); however, nitrate (NO_3^-), one of the major forms of fixed N, is also a powerful oxidant. Laboratory studies have recently identified bacteria that can mediate both Fe(II) (6–8) and As(III) (9) oxidation by NO_3^- , and field evidence suggests that NO_3^- may influence Fe cycling in natural systems (10–13). Here we show that NO_3^- is dominant in the control of both As and Fe cycling during anoxia in urban, seasonally stratified, and eutrophic Upper Mystic Lake (UML; maximum depth ~ 24 m, surface area ~ 50 ha, volume ~ $7 \times 10^6 \text{ m}^3$). The results have

implications for element cycles in many N-polluted aquatic systems.

UML's sediments contain 200 to 2100 parts per million (ppm) of As, derived primarily from industrial activity (14). These sediments are a seasonal source of As to the water column (15–17). Conventionally, the presence or absence of O_2 is considered the main determinant of Fe (10) and As (18) chemistry in nonsulfidic lake waters (19), and anoxia does initiate release of Fe and As from UML sediments into the hypolimnion (depths ~ 10 to 24 m). However, the expected reduced chemical forms, As(III) and dissolved Fe(II) (19), have only materialized occasionally in UML (15). Instead, oxidized As and particulate Fe(III) have accumulated in the anoxic water column during most years (16, 17, 20). For example, by late July 1997, O_2 had fallen below detection limits (~5 μM) in waters deeper than 15 m, and Fe and As began to be released from the sediments (Fig. 1, A and B) (21). Fe(II) and As(III), however, represented only small percentages of total As and Fe throughout the following 4 months of anoxia. Because the Fe must have been remobilized from the sediments in soluble form as Fe(II), most of this Fe was oxidized subsequent to release, in the absence of O_2 . Similarly, any As remobilized as As(III) must have been anaerobically oxidized to As(V).

We hypothesized that NO_3^- was responsible for the dominance of oxidized Fe and As. In UML, as in many eutrophic lakes, NO_3^- levels (21) frequently exceed 100 μM (Fig. 2). Persisting for several months after seasonal thermal stratification (thermocline at depth of 7 m) and subsequent O_2 depletion in UML, a large fraction of the NO_3^- pool was produced in situ through microbial oxidation of NH_4^+ (i.e., nitrification).

Parsons Laboratory, Department of Civil and Environmental Engineering, Massachusetts Institute of Technology, Cambridge, MA 02139, USA.

*Present address: Department of Environmental Science and Engineering, Harvard School of Public Health, Building 1 Room G21, 665 Huntington Avenue, Boston, MA 02115, USA.

†To whom correspondence should be addressed. E-mail: dbsenn@alum.mit.edu